Communications

Simultaneous Concentration and Separation of Proteins in a Nanochannel**

David W. Inglis, Ewa M. Goldys, and Nils P. Calander*

Molecular separation technologies, such as gel electrophoresis and liquid chromatography coupled with mass spectrometry detection, have been the foundations of biomarker discovery. This is because medically significant biomarkers, for example in blood, can be as much as 10^{12}-fold less common than the most abundant protein, albumin, and detecting these low-abundance molecules requires high sensitivity and selective depletion of the dominant species.[1] Conventional approaches, including antibody depletion, remove selected molecules by less than three orders of magnitude only. This limitation prevents the isolation, characterization, and discovery of millions of new proteins where key disease markers could be identified.[1] Overcoming this barrier requires new approaches to analytical detection that minimize sample preprocessing steps while achieving high throughput with very high levels of sensitivity.

Here we describe a new device that demonstrates simultaneous concentration and separation of proteins by conductivity gradient focusing. Concentration and separation take place in an electric-field-driven 120 nm deep nanochannel that supports a stable salt and conductivity gradient.

Conductivity gradient focusing is one of many techniques that use opposing convective flow and electrophoretic forces to focus molecules to an equilibrium position. These methods include a step change in chromatographic packings,[2] electrochromatography,[3] varying the molecular charge (as in isoelectric focusing), temperature gradient focusing,[4] varying the cross-section through which the electric current flows,[5] and varying the buffer conductivity.[6] In contrast to all of these approaches, the device presented herein does not require ampholytes, matrices or gels, membranes, temperature gradients, or an external pump.

Electrokinetic phenomena at the nanoscale have recently been shown to produce a rapid and high preconcentration[7–19] of proteins and peptides in physiological buffers. In these reports, nanochannels in microfluidic devices create gradients in the electric field by their charge-selective transport characteristics. By combining this with a transport mecha-

nism, often electro-osmosis, charged molecules can be trapped and accumulated owing to a balance in the viscous drag force and the electrophoretic force. The interaction of surface charges, mobile charges, and water molecules with each other and the electric field is complex, but our understanding has been advanced by a number of excellent fundamental studies.[16–19] Concentration polarization, as it is sometimes known, at the entrance to a nanochannel gives rise to a gradient in the concentration of salt ions, which in turn perturbs the electric field, thereby creating a trap. Typically, these traps cause sample stacking on the microchannel side of the microchannel to nanochannel junction. In such cases, the electric field gradient is very abrupt, causing all molecules to accumulate in a tightly confined region, with limited scope for separation.

Recent experiments[7–21] are primarily concerned with preconcentration only, which may increase the detection sensitivity of trace analytes in purified solutions. However, when analytes such as protein biomarkers are found in complex media such as blood plasma, preconcentration alone is unlikely to improve their detectability.

Our work is based on the idea that, by placing the gradient and the molecules in the nanochannel, the gradient is extended, thus allowing separation of molecules while they are being concentrated. This method makes it possible to demonstrate, for the first time, the feasibility of simultaneous concentration and separation of proteins in a nanofluidic channel. Furthermore, rather than relying on concentration polarization, we use a nanochannel that connects a high conductivity and a low conductivity microchannel to impose an electric field gradient. The experimental results are supported by numerical modeling that accurately predicts trap locations and accumulation speed. High concentration factors, fast accumulation rates, and the compactness of the device make it well-suited to integration into microfluidic systems where more detailed downstream analysis can take place.

Balancing the electrophoretic and viscous drag forces requires a spatial variation (gradient) of at least one of these forces. Herein, we create a gradient in the electrophoretic force (electric field) by establishing a conductivity (salt concentration) gradient along the nanochannel that connects the high-concentration and low-concentration salt reservoirs (high- and low-salt; Figure 1). When an electric field is applied, an electro-osmotic flow resulting from negative surface charge carries the high-salt solution through the nanochannel, but the low-salt reservoir determines the salt concentration at one end. This effect leads to a sharp gradient in salt concentration, electrical conductivity, and electric field near the low-salt end of the nanochannel (Figure 1c). Trap-

[*] Dr. D. W. Inglis, Prof. E. M. Goldys, Dr. N. P. Calander
Department of Physics and Astronomy, Macquarie University
Sydney, NSW 2109 (Australia)
E-mail: david.inglis@mq.edu.au

Supporting information for this article is available on the WWW under http://dx.doi.org/10.1002/anie.201100236.
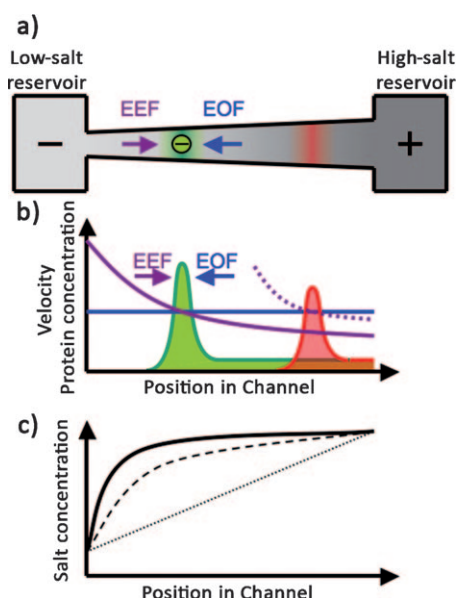
Figure 1. The fundamental concepts of conductivity gradient focusing. a) A conductivity gradient is established in a nanochannel connecting two reservoirs. At the high-concentration salt (high-salt) side, the electro-osmotic force dominates (blue arrow), while at the low-salt side the electrophoretic force dominates (purple arrow). b) Proteins (green and red) are trapped wherever the net force is zero. This point depends on mobility. c) Salt concentration as a function of position in the channel. The high-salt solution is pushed through the channel by electro-osmotic flow, but it is forced to the low-concentration salt value at the end of the nanochannel, leading to a sharp gradient near the low-salt end. The device reaches a stationary salt concentration gradient shortly after the electric field is applied at $t = 0$ (•••••). Also shown: $t = 10$ s (-----), $t = \infty$ (——) (simulated).

Figure 2. Device description. a) Cross-section of the device showing a 120 nm-deep nanochannel. b) Top view of the nanochannels (purple) connecting two microchannels. The four vertical lines are microchannel edges. c) Top view of the entire device. The four dark circles (one is obscured) are holes cut through the silicon for liquid and electrode access.

ping of charged analyte molecules is achieved at points along the channel where the net velocity of a molecule is zero, and the velocity gradient is negative. The location of the trap depends on the electrophoretic mobility of the molecular species. Molecules with higher mobility (charge-to-size ratio) are captured at positions closer to the high-salt side, whereas molecules with lower mobilities are trapped closer to the low-salt end (Figure 1 a). This behavior gives rise to simultaneous concentration and separation of molecular species with different electrophoretic mobilities.

Figure 2 shows various views of the device, which comprises a pair of 8.6 μm-deep microchannels connected by 25 parallel nanochannels, each 120 nm deep and 500 um long. The nanochannels are 62 μm wide at the right end and 22 μm wide at the left, with a 2° half-angle. Low- and high-salt buffers are continuously transported through the left and right microchannel, respectively. The proteins under investigation are added to the right-hand, high-salt microchannel. Capillary forces and evaporation at the downstream end continuously drive the fluid in the microchannels at approximately 100 μm s^{-1} (5 nL min^{-1}). This flow sustains the salt concentration gradient despite the buffer exchange through the nanochannels. A positive voltage is applied to electrodes in the right-hand, high-salt microchannel, while the left-hand, low-salt channel is grounded. Electro-osmotic flow carries the buffer with dissolved proteins into the nanochannel, where
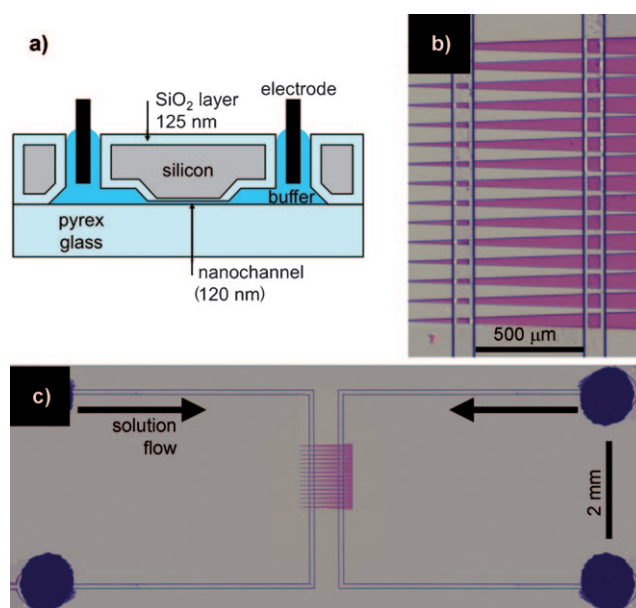
they may be trapped. The presence of the protein does not affect the gradient, as the bulk protein concentration is much less than the salt concentration.

Here, we demonstrate simultaneous concentration and separation of R-phycoerythrin (R-PE) and Dylight488-labelled streptavidin (Dyl-Strep), with molecular weights of 240 and 54 kDa, respectively (Figure 3). Initially, the two proteins are mixed in the right-hand, high-salt microchannel (0.78 μM Dyl-Strep, 33 nM R-PE in 141 mM NaCl PBS, pH 7.8, conductivity 15.5 mS cm^{-1}). The left-hand, low-salt microchannel carries a 20-fold dilution of phosphate buffered saline (PBS; 7 mM) with a conductivity of 0.87 mS cm^{-1}. The two proteins are well-resolved ($R = 1$) after 110 seconds with an applied voltage of 4 V (Figure 3 a,b). The R-PE molecules have been concentrated by a factor of 60 and the Dyl-Strep molecules by a factor of 51. Concentration enhancement is calculated as the peak intensity divided by the microchannel intensity times a geometric factor that corrects the fluorescence intensity for the depths of the microchannels and nanochannels.

The trap location as a function of protein mobility can be determined from our numerical model (Figure 3 c; see the Supporting Information for details). The model uses the geometry and salt concentrations as in the experiment. The experimental peak positions from Figure 3 a and b are shown in Figure 3 c as red and green lines; the model predicts molecules trapped at these positions to have mobility values of −1.23 and −0.98 μm cm V^{-1} s^{-1} for the R-PE and Dyl-Strep molecules, respectively.

We now discuss if the values of parameters in the model are consistent with the properties of the proteins. To this aim
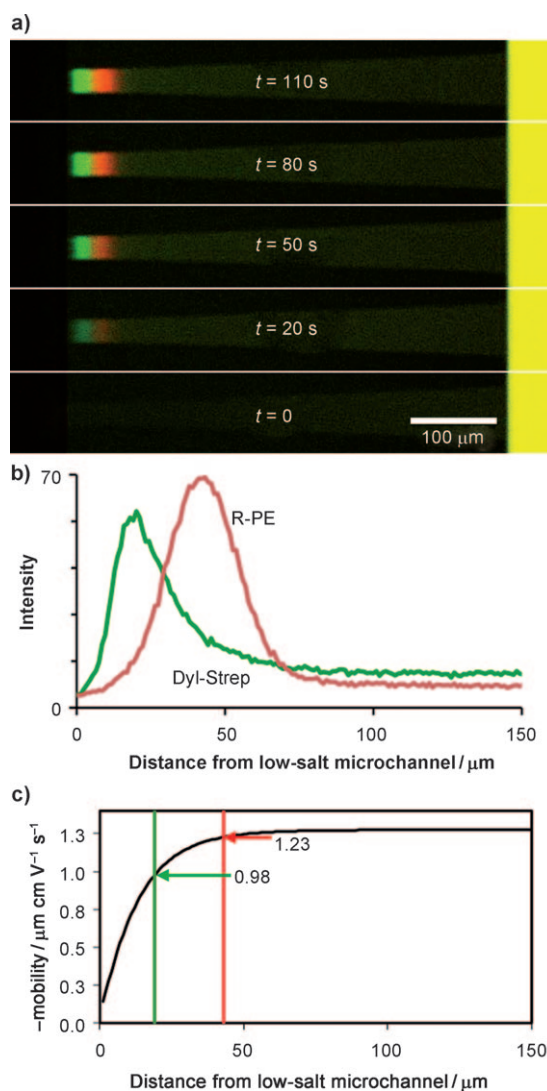
Figure 3. Simultaneous concentration and separation of proteins. a) Top-view fluorescence image of the device operated at 4 V after 110 seconds. Two molecules, R-PE (red band) and Dyl-Strep (green band) are initially mixed in the high-salt microchannel on the right (yellow stripe). They flow into the nanochannel where they are concentrated and separated into two clearly resolved bands near the low-salt end. (For a time-lapse movie of this process, see the Supporting Information.) b) Fluorescence intensity as a function of position in the channel of the two labeled proteins from (a). c) Our model prediction of trap position as a function of protein mobility. Green and red lines mark the experimental positions of the two proteins from which their mobility can be extracted (see the text for details).

we measured protein mobility, hydrodynamic size, and effective charge by combined methods of dynamic light scattering and AC electrophoresis using a Malvern Zetasizer. The measurements of effective protein charge (−8.5*e* and −2.3*e* for R-PE and Dyl-Strep, respectively, where *e* denotes elementary charge) compare well with those obtained using the individual pH dependent contributions from amino acids and, in the case of Dyl-Strep, the fluorescent label: −12*e* and −4.4*e*. The measured physical diameters are 7.8 ± 2.0 nm and

4.9 ± 1.4 nm, while the diameter of the proteins from the RCSB Protein Data Bank[22] are 7.6 and 5.0 nm.

The measured values of mobility were $-1.8 \pm 0.6 \ \mu m \, cm \, V^{-1} s^{-1}$ and $-0.8 \pm 0.9 \ \mu m \, cm \, V^{-1} s^{-1}$, for R-PE and Dyl-Strep, respectively. The corresponding nanofluidic device predictions of mobility, $1.23 \ \mu m \, cm \, V^{-1} s^{-1}$ and $0.98 \ \mu m \, cm \, V^{-1} s^{-1}$, are consistent with these measurements. The values of surface charge density, σ, used in the models, $80\,000 \ e \, \mu m^{-2}$ and $35\,000 \ e \, \mu m^{-2}$, are in agreement with values found in the literature.[19,24]
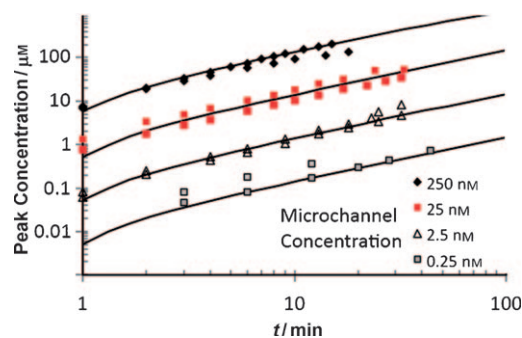

Figure 4. Protein (R-phycoerytrin) concentration as a function of time. Data points are experimental results using the protein R-PE at initial microchannel concentrations of 0.25, 2.5, 25, and 250 nM. Solid lines are results of our modeling ($\sigma = 35\,000 \ e \, \mu m^2$). After 17 min at 4 V, the protein concentration increases by a factor of 1000.

Regarding the accumulation rate of molecules in a trap (Figure 4), we examined the accumulation of R-PE from initial concentrations spanning 4 orders of magnitude (0.25 nM to 250 nM). After an initial delay, owing to time it takes for molecules to arrive at the trap, their concentration increases very rapidly. Later, when the concentration in the trap becomes much larger than the bulk concentration, the growth rate becomes linear. The model predicts that 1000-fold concentration enhancement is reached in 16.8 minutes, which is in good agreement with a value of 17 ± 7 min observed experimentally. The accumulation rate is independent of protein concentration, provided the charge contributed by the accumulated protein is insignificant when compared to the salt concentration along the nanochannel (> 7 mM). Thus, given enough time, protein molecules can be concentrated from an arbitrarily low initial concentration to a maximum concentration that is eventually limited by the salt concentration. The accumulation rate is determined by the arrival rate of molecules entering the nanochannel from the reservoir, which is strongly affected by the applied voltage.

Our method separates proteins by electrophoretic mobility. To predict how other proteins will behave in this type of device, protein mobility could be estimated as the ratio of effective charge to effective radius divided by the Stokes drag coefficient, $6\pi\eta$, where η is viscosity.[25] Protein charge and radius obtained from protein structure calculations may be used as a preliminary guide; however, they neglect the effect of the buffer, which decreases effective charge owing to

screening and also increases in size owing to the Stern layer and protein folding. Therefore, actual mobility measurements are more accurate than the estimates based on information from the protein databases.

This work demonstrates separation of the two proteins, whose electrophoretic mobility differs by a factor of approximately 1.8, with a resolution R of 1 and concentration enhancement of 1000 in approximately 17 minutes in a nanochannel. The experimental results are interpreted by a complete modeling of electric, electrophoretic, and hydrodynamic effects. Our results are significant because analytical biotechnology requires detection of molecules in mixtures where molecular components span an enormous range of concentration. The results demonstrated show that, with appropriate optimization of the electric field gradient, relevant proteins can be concentrated to detectable levels while these insufficiently removed and obscuring species will be separated. This method will provide new windows for yet unknown proteins to be revealed, concentrated, and analyzed downstream by other methods, such as mass spectrometry, thus advancing the field of biomarker discovery.

Experimental Section

Devices were fabricated using standard semiconductor techniques. Microchannels were photolithographically patterned on 3'', p-type 5–10 Ohm cm wafers with 50 nm of thermal oxide followed by CF_4/O_2 plasma etching. A 50-μm layer of SU-8 resist was then used to protect the wafers during sandblasting of holes for back-side fluid and electrode ports. Sequential cleaning in detergent, acetone, and Remover PG (Microchem Corp., Newton MA USA) was performed to remove sand particles, SU-8, and photoresist. Clean wafers were then etched for 23 min in a stirred, 70°C solution of 14% w/v potassium hydroxide and 17% v/v isopropyl alcohol. After etching to 8.6 μm, the remaining oxide was removed by hydrofluoric acid, and 110 nm of new thermal oxide was grown to isolate the fluidic channels from the silicon. Nanochannels connecting the pair of microchannels were patterned and etched to a depth of 120 nm by photolithography, followed by CF_4/O_2 plasma etching. Pyrex wafers were bonded to these silicon wafers using the reverse RCA procedure; 10 min piranha ($H_2SO_4/30\%$ H_2O_2 4:1 v/v), 5 min RCA2 (70°C, 37% HCl/30% H_2O_2/H_2O 1:1:6 v/v), 5 min RCA1 (70°C, 29% $NH_4O_4/30\%$ H_2O_2/H_2O 1:1:5 v/v). Between each step the wafers were rinsed thoroughly in running deionized water. The sealed wafers were bonded by annealing at 350°C for 12 h.

Devices were run on a Leica DM-IRB inverted microscope with SP-2 confocal imaging capabilities. The two proteins were imaged using the 488 nm laser and two spectral windows that led to no crossover: 505–545 nm for Dyl-Strep and 582–603 nm for R-PE. For a quantitive determination of R-PE intensity in Figure 4, images were taken using a 12-bit high-sensitivity digital camera (Nikon DS-Qi1Mc) and a mercury lamp.

Protein mobility measurements and calculations: R-Phycoerythrin (Supporting Information, Figure S3) is 9 nm by 6 nm and roughly rod-shaped.[18] The total charge can be calculated by adding the charges of the various charged amino acids versus pH (Supporting Information, Figure S4). At pH 7.8, the charge is −12 elementary charges. For comparison, the Protein Dipole Moments Server[23] gives a charge of −8 elementary charges at pH 7. R-PE was supplied by AnaSpec Inc., California. We measured a diameter of 7.8 ± 2.0 nm by dynamic light scattering in 20 mM NaCl PBS. We also measured a mobility of -1.8 ± 0.6 μm cm $V^{-1} s^{-1}$ using a Malvern Zetasizer. The charge is calculated from these two measured quantities by multi-

plying the mobility by the Stokes drag coefficient for a sphere of diameter 7.8 nm. The resulting charge is −8.5 elementary charges.

Streptavidin (Supporting Information, Figure S5) is circular and is about 5 nm in diameter.[18] The total charge was calculated by adding the charges of the various charged amino acids versus pH (Supporting Information, Figure S6). At pH 7.8, the charge is −4.2 elementary charges. The Protein Dipole Moments Server[23] gives a charge of zero electrons at pH 7. The Dylight488 molecule has an insignificant mass of 826 g mol^{-1}, but a net charge of one electron (Supporting Information, Figure S7). The manufacturer claims an average of 2.2 labels per streptavidin protein molecule, so we estimate the total molecular charge at pH 7.8 to be −6.4 elementary charges. Dylight488-streptavidin was supplied by Jackson Immuno-Research. We measured a diameter of 4.9 ± 1.4 nm by dynamic light scattering in 20 mM NaCl phosphate buffered saline (PBS). We also measured a mobility of -0.8 ± 0.9 μm cm $V^{-1} s^{-1}$ using a Malvern Zetasizer. The charge is calculated from these two measured quantities by multiplying the mobility by the Stokes drag coefficient for a sphere of diameter 4.9 nm. The resulting charge is −2.3 elementary charges.

The theoretical model used here is based on the Poisson–Nernst–Planck equation (describing the concentration and motion of the salt ions and the negatively charged analyte molecules) and the Navier–Stokes equation (concerned with the liquid flow). The finite element method (FEM) and the program COMSOL V3.5a (Boston, MA) are used to solve the equations using appropriate boundary conditions. These include specified concentrations of the salt (NaCl) and analyte, electric potential, and pressure within the reservoirs. Channel walls are impermeable to ions, molecules, and water, and we used a surface-charge boundary condition for the electric field at the channel walls. The model, including all physical parameters used, is described more fully in the Supporting Information.

[1] V. Polaskova, A. Kapur, A. Khan, M. P. Molloy, M. S. Baker, *Electrophoresis* **2010**, *31*, 471–482.
[2] P. H. O'Farrel, *Science* **1985**, *227*, 1586.
[3] S. K. Basak, A. Velayudhan, K. Kohlmann, M. R. Ladisch, *J. Chromatogr. A* **1995**, *707*, 69–76.
[4] D. Ross, L. E. Locascio, *Anal. Chem.* **2002**, *74*, 2556–2564.
[5] W. S. Koegler, C. F. Ivory, *J. Chromatogr. A* **1996**, *726*, 229–236.
[6] R. D. Greenlee, C. F. Ivory, *Biotechnol. Prog.* **1998**, *14*, 300–309.
[7] K. D. Huang, R. J. Yang, *Electrophoresis* **2008**, *29*, 4862–4870.
[8] K. C. Kelly, S. A. Miller, A. T. Timperman, *Anal. Chem.* **2009**, *81*, 732–738.
[9] Y. Wang, K. Pant, Z. Chen, G. Wang, W. F. Diffey, P. Ashley, S. Sundaram, *Microfluid. Nanofluid.* **2009**, *7*, 683–696.
[10] Y. C. Wang, A. L. Stevens, J. Y. Han, *Anal. Chem.* **2005**, *77*, 4293–4299.
[11] Y. C. Wang, J. Y. Han, *Lab Chip* **2008**, *8*, 392–394.
[12] D. Hlushkou, R. Dhopeshwarkar, R. M. Crooks, U. Tallarek, *Lab Chip* **2008**, *8*, 1153–1162.
[13] K. M. Zhou, M. L. Kovarik, S. C. Jacobson, *J. Am. Chem. Soc.* **2008**, *130*, 8614–8616.
[14] D. P. Wu, A. J. Steckl, *Lab Chip* **2009**, *9*, 1890–1896.
[15] R. W. Clarke, S. S. White, D. J. Zhou, L. M. Ying, D. Klenerman, *Angew. Chem.* **2005**, *117*, 3813–3816; *Angew. Chem. Int. Ed.* **2005**, *44*, 3747–3750.
[16] N. Calander, *Anal. Chem.* **2009**, *81*, 8347–8353.
[17] A. Plecis, C. Nanteuil, A. M. Haghiri-Gosnet, Y. Chen, *Anal. Chem.* **2008**, *80*, 9542–9550.

[18] A. Mani, T. A. Zangle, J. G. Santiago, *Langmuir* **2009**, *25*, 3898–3908.

[19] A. Mani, T. A. Zangle, J. G. Santiago, *Langmuir* **2009**, *25*, 3909–3916.

[20] J. G. Shackman, D. Ross, *Electrophoresis* **2007**, *28*, 556–571.

[21] X. F. Sun, D. Li, A. T. Woolley, P. B. Farnsworth, H. D. Tolley, K. F. Warnick, M. L. Lee, *J. Chromatogr. A* **2009**, *1216*, 6532–6538.

[22] Protein Data Bank (PDB): http://www.rcsb.org

[23] Protein Dipole Moments Server: http://bioinfo.weizmann.ac.il/dipol/

[24] S. H. Behrens, D. G. Grier, *J. Chem. Phys.* **2001**, *115*, 6716–6721.

[25] H. C. Ber, *Random Walks in Biology*, Princeton University Press, **1983**.